MODELING OF HEAT LOADS ON THE JET DIVERTOR DURING EDGE LOCALIZED MODES

F. Subba[(1)], F. Turco[(1)], R. Zanino[(1)]

[(1)]Dipartimento di Energetica, Politecnico, Corso Duca degli Abruzzi 24, 10129Torino, fabio.subba@polito.it

ABSTRACT

We analyse the impact of Edge Localize Mode (ELM) events on the target plates of the JET tokamak. ELMs transfer into the Scrape-off Layer a fraction of the confined plasma energy, producing transient thermal loads on the solid structures of several hundreds of MW/m^2, which can severely damage the solid plasma facing components. We study numerically an ELM in JET using the SOLPS B2-Eirene code, and compare our results with the available experimental data, with emphasis on the description of the heat loads on the divertor targets. The major current uncertainty sources for computational modelling are also briefly discussed.

1. INTRODUCTION

The *International Thermonuclear Experimental Reactor* (ITER) should to operate in the so-called ELMy H-mode [1]. The intermittent *Edge Localized Modes* (ELMs) should extract from the plasma the exhausted fuel, while preserving the attractive confinement properties of the H-mode. However, ELMs can represent a serious engineering concern. For typical values of the experiment EFDA-JET (Culham, UK) a medium-size ELM releases a few hundreds kilojoules in a few microseconds. The resulting peak thermal loads onto the solid walls are as high as some hundreds of MW/m^2. The corresponding expected values for ITER are even larger [2, 3]. Such a power deposition can increase, even if for a short time, the surface temperature above the technological limit, shortening the life of the plasma-facing components.

Numerical modelling should help understanding the impact of ELMs on the exposed solid surfaces, contributing to an optimised design of the plasma facing components. On the other hand, it is known that modelling accurately the transient evolution of a burst of plasma entering the SOL abruptly is very challenging [4, 5]. In this paper we apply the SOLPS B2-Eirene code [6] to simulate a medium-size ELM in JET. In section 2 we introduce the physical model and the solution technique, in section 3 we present our results for the quiescent inter-ELM phase and during the ELM transient, with emphasis on the heat loads on the target plates. In section 4 we draw our conclusions.

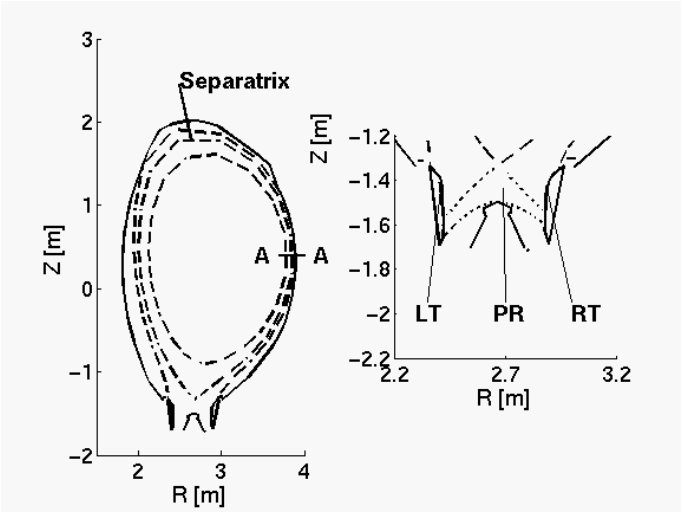

Figure **1**. Right: representation of the JET tokamak. The solid lines are the components of the vessel. The innermost and outermost dashed lines define the computational domain used in this paper. The central dashed line is the *magnetic separatrix*. AA is called the *outer mid-plane* section. Right: zoom of the d*ivertor region*. LT and RT mark the *left* and the *right target*, PF the *Privte Flux* region.

2. MODEL DESCRIPTION

Geometry and Model Equations

Since tokamaks are axi-symmetric, a cross-section on a vertical plane including the symmetry axis (*Z*) provides

the simplest, 2D, geometrical model. Such a representation is called a *poloidal cross section*. Figure 1 shows the poloidal cross section of JET (solid lines). The magnetic field lays on a set of nested *magnetic surfaces* (dashed). The innermost and outermost magnetic surfaces represented in the figure are the boundaries of the simulated domain. The central one is the *separatrix*. It divides the inner region, the *main plasma*, from the *Scrape-off Layer* (SOL) where the field lines intersect the solid boundaries. The SOL portion below the separatrix is called the *private region*. Most of the plasma-wall interactions are concentrated at the *Left Target* (LT) and at the *Right Target* (RT).

The description of tokamak plasma must allow at least for the presence of the electrons, of a number of ion species, and of the neutral particles. In addition, the electric field must be computed self-consistently with the evolution of the plasma species. Since changes in the (equilibrium) magnetic field are far slower than the plasma dynamics, we treat it as fixed. The magnetic field map is computed during the pre-processing phase, based on the solution of the Grad-Shafranov equation [7]. For the plasma components, we adopt a widely used fluid model proposed by Braginskii in the 60th [8].

Experimental data [9] show that the Braginskii model is reasonably accurate on the magnetic surfaces, but fails to reproduce plasma transport in the third (*radial*) direction. However, the radial thermal fluxes play a crucial role in determining the loads on the vessel components, and must be accurately reproduced. Then, we adopt phenomenological mass and energy diffusion laws in the radial direction. The system of equations solved is:

$$\frac{\partial n^i}{\partial t} + \nabla \cdot \overline{\Gamma}^i = S^i \tag{1}$$

$$n^e = n^i \tag{2}$$

$$\frac{\partial \left(m^i \Gamma^i_{//} \right)}{\partial t} + \nabla \cdot \left(m^i \Gamma^i_{//} \overline{V}^i + p\hat{I} - \hat{\eta}^i \cdot \nabla V^i_{//} \right) = S^{\Gamma,i} \tag{3}$$

$$\frac{\partial}{\partial t}\left(\frac{3}{2} n^i T^i + \frac{1}{2} m^i n^i \left(V^i_{//} \right)^2 \right) + \nabla \cdot \overline{q}^i = S^{E,i} \tag{4}$$

$$\frac{\partial}{\partial t}\left(\frac{3}{2} n^e T^e \right) + \nabla \cdot \overline{q}^e = S^{E,e} \tag{5}$$

$$\nabla \cdot \bar{j} = 0 \tag{6}$$

(symbols are defined in section 6).

Equation (1) is the ion continuity equation. Equation (2), called the *quasi-neutrality* relation, is an approximation satisfied on spatial scales larger than the Debye length [7]. It states that the plasma does not develop any large-scale charge-separation. It is valid because charge-separations in the plasma are opposed by strong electric fields. Equation (3) is the projection of the ion momentum equation along $\overline{B}$. The other two components are approximated by a diffusion-type law. Note that Eq. (3) involves the total pressure, i.e. the sum of the ion and electron contributions. It can be shown that the electron term accounts for the electric force acting on the ions. Equations (4) and (5) are the energy equations for ions and electrons, respectively. (Note: in the following we will always express the temperatures in eV units). The kinetic energy of electrons is omitted, because of their small mass. In spite of their apparent simplicity, the heat fluxes are tensor quantities, and their expression is quite involved [8, 10]. Finally, Eq. (6) is the charge-conservation relation. Equations (1)-(6) with the two additional diffusive relations form a system in the 8 variables n^i, n^e, $\overline{\Gamma}^i$, T^i, T^e, and the electrostatic potential j [7, 8]. The sources of Eq. (1)-(6) describe the interaction of the plasma with the neutral particles, which require an additional model for their evolution. Due to the low neutral density in the tokamak plasma, the kinetic approach is often needed, and we solve a Boltzmann equation for each neutral particle species.

We wrote Eq. (1)-(6) for the case of a 2-component plasma for the sake of simplicity, but they can be generalized to the multi-species case [11]. In what follows, we consider a plasma composed by electrons, deuterium and the six ionisation stages of carbon.

Boundary Conditions.

We fix the boundary conditions taking the best possible advantage of the available experimental information. Unfortunately, the problem of getting reliable data from tokamak plasma is a formidable one. We do not enter in the details of this large and evolving field [9]. As a thumb rule, we say that experimental data with more than 20% accuracy can be considered very good, but most of the times data affected by an error up to a factor 2 are not surprising. For our purposes, all the not (or only partially) known information on the system introduce a number of free parameters, which influence the final result. As a consequence, successfully modelling of tokamak plasma largely depends on the modeller experience and physical intuition. We illustrate here the physical reasons leading to our choice of boundary conditions.

Particle balance. At the inner plasma boundary we fix the particle influx. This must account for: (i) the high temperature neutral beams injected purposely in the core plasma to heat it (NBI), and (ii) the neutrals which, coming from the SOL, penetrate in the core plasma, ionise by collision with the electrons and diffuse back into the computational domain. At the other boundaries, the ions striking the solid walls recombine to form neutral molecules and recycle into the plasma with a certain probability, defined by the conditions of the vessel surface. An ion hitting the wall has also a finite probability of extracting an atom from the solid surface

(*sputtering*). This provides the main impurities source for the plasma. Since the JET vessel is made of graphite, we assume carbon is the only impurity species. Uncertainties in the sputtering yields are introduced by the unknown morphological state of the solid surface. At the bottom of the vessel, a pumping system extracts neutral gas molecules from the divertor region. We model it by reducing locally the recycling probability. Finally, we inject from the top a constant rate of deuterium atoms, to model the gas puff system used to fuel the plasma.

Energy balance. We fix the energy flux into the plasma at the inner boundary. The NBI system supplies the external power source. Some power is deposited in the core plasma (which is heating-up during the inter-ELM phase), or is radiated by the impurities. The quantitative importance of the last two contributions is difficult to evaluate. As a consequence, it is not clear *a priori* what power enters the computational domain: we can only estimate it *a posteriori*.

Momentum balance. This is the most uncertain boundary condition in our modelling, due to uncomplete experimental information. We impose tentatively zero plasma velocity along $\overline{B}$ at all boundaries except the targets, where theoretical analysis suggests to set an outgoing velocity equal to the ion sound speed [9]. Preliminary analysis suggests that this assumption is not critical for the results we are going to discuss. A deeper analysis of the momentum balance is currently going on, but is not presented here.

Charge balance. The target currents are determined self-consistently according to the sheath theory [9]. No current is assumed to cross the other boundaries.

Solution Method.

Eq. (1)-(6) are solved using the Finite Volume method on a grid with 12 volumes in the radial direction, and 48 along the magnetic surfaces [12], while we deal with the Boltzmann equation for the neutrals using a time-dependent Monte-Carlo solver [13]. The details of the solution method are as follows. Let us assume that the status of the plasma neutrals at the time $t = t^k$ is given. First the plasma system, Eqs. (1)-(6), is advanced to $t = t^{k+1}$ by the B2 code with an implicit scheme. The new plasma fluxes at the boundaries, and the full 2D maps of densities, velocities and temperatures are passed to the Monte-Carlo solver (Eirene). Then, Eirene solves the Boltzmann equation in the interval $t^k \le t \le t^{k+1}$. Sources due to surface and volumetric processes are determined using the plasma data at time $t = t^{k+1}$. After that, Eirene re-computes the values of the collision sources with the updated neutral distribution, and returns them to B2 for a new time step.

As we see, the plasma (fluid) and neutral (kinetic) equations are explicitly coupled trough the source terms. In principle, this could engender numerical instabilities if too large time steps were used.

Actually, the strongest constraint on the time step is determined by the need to resolve the neutral dynamics correctly. The average neutral lifetime is determined by ionising collisions. We estimate it assuming $n^e \approx 2\times10^{19}\,\mathrm{m}^{-3}$, and $T^e \approx 100\,\mathrm{eV}$ (values at the separatrix, characteristic of the experiment we studied during the inter-ELM phase). Then the ionisation time of a deuterium atom can be estimated as $t_{ion} \ge 10^{-6}\,\mathrm{s}$ [9], which provides an upper estimate for the required time step.

We model first the inter-ELM phase with a steady-state plasma, to produce an initial condition for the transient. Although this approach is not strictly correct, since the plasma before an ELM is not fully steady state, this method is justified because the plasma evolution following the ELM is much faster than during the preceding quiescent phase.

Transport coefficients

As previously mentioned, our understanding of radial transport in tokamaks is not complete. As a consequence, transport coefficients must be deduced by comparison with experimental data. We tuned the particles and energy diffusivities in order to match the inter-ELM density and temperature radial profiles with the corresponding measurements.

Figure 2 show the radial profiles of D and c along the outer mid-plane section. The low values at the separatrix are characteristic of the H-mode, and are probably

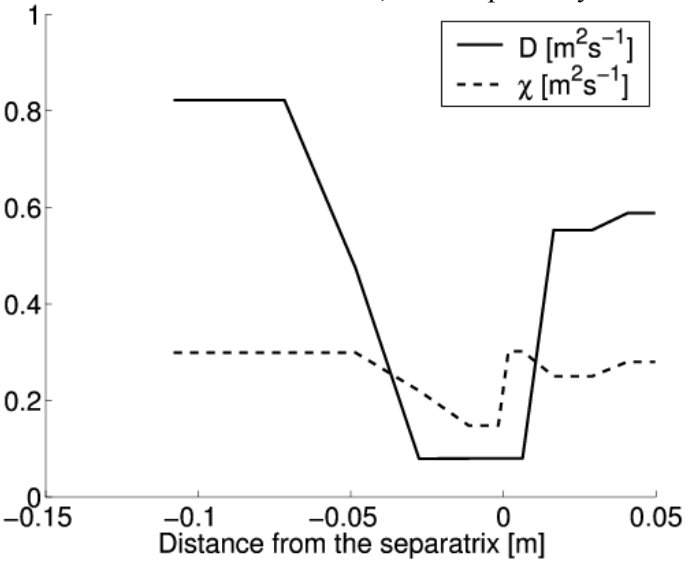

Figure 2. Radial profiles of the particle (D) and thermal (χ) diffusivities used for the modeling of the quasi steady-state inter-ELM phase.

connected to the radial electric field properties [14]. The orders of magnitude are consistent with the experience of the fusion community [9], but the detailed shape depends on a fit process to the experimental data.

Roughly speaking, an ELM is an instability, which destroys for a few hundred microseconds the structure of the magnetic field, connecting directly the main plasma with the SOL [15]. During this time, a large number of hot particles can flow into the SOL, and then down to the target.

In our modelling, we triggered an ELM by temporarily

increasing the radial diffusivities D and c around the separatrix. As a general guideline, we tried to stay as close as possible to the experimental estimates of the duration of the trigger event, and the energy and particles losses from the confined plasma.

3. RESULTS

We discuss here the results of our study. We will concentrate on a case with 3.6×10^{21} s^{-1} D^+ ions injected from the plasma boundary, 5.1×10^{21} s^{-1} D atoms puffed from the top and 6.5 MW input power. These conditions are kept for both the inter-ELM and the transient phase. Their validity during an ELM is somewhat doubtful. We kept them anyway: partly for the sake of simplicity, and partly based on the argument that the plasma, sufficiently deep inside the separatrix, should be relatively unaffected by the ELM. Part of the following analysis is based on preliminary results from the JET Infrared Camera, which were kindly provided by Dr. T. Eich (IPP-Garching).

Steady state

Figure 3 compares the computed density profiles for electrons and C^{6+} ions at the outer mid-plane with the experimental data. The C^{6+} values have been multiplied by a factor 20, to be visible on the scale of the figure. We do not have direct measurements for the other

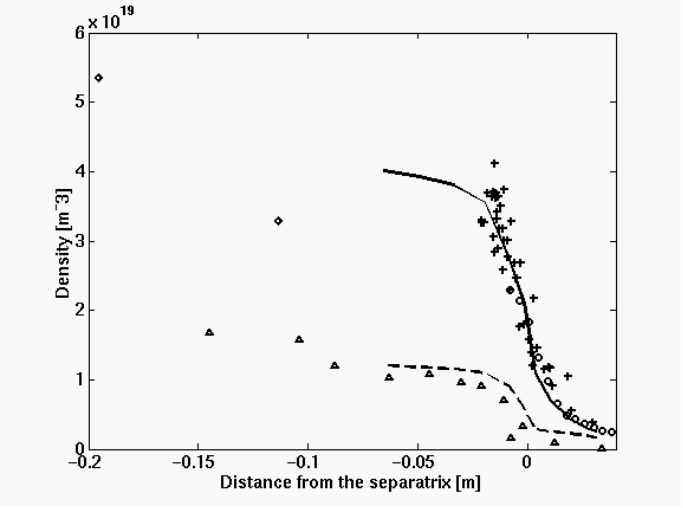

Figure 3. Density profiles of electrons and fully ionized carbon from numerical modeling and different experimental diagnostics. The traces for electrons are: (+) edge lidar, (o) lithium beam, (□) line averaged lidar, and (□) numerical model, the carbon traces are: (□) charge exchange, and (--) numerical model. The carbon traces have been multiplied by a factor 20 to be visible on the figure scale.

ionisation stages. However, since the presence of C^{6+} in the plasma depends on a chain of processes, which starts with the C^0 sputtered from the solid wall [9], we expect our computations to be at least as accurate for the lower ionisation stages as for C^{6+}.

Figure 4 shows the temperature profiles at the mid-plane section. We show measurements of T_e and T_i together because ions and electrons should be thermally

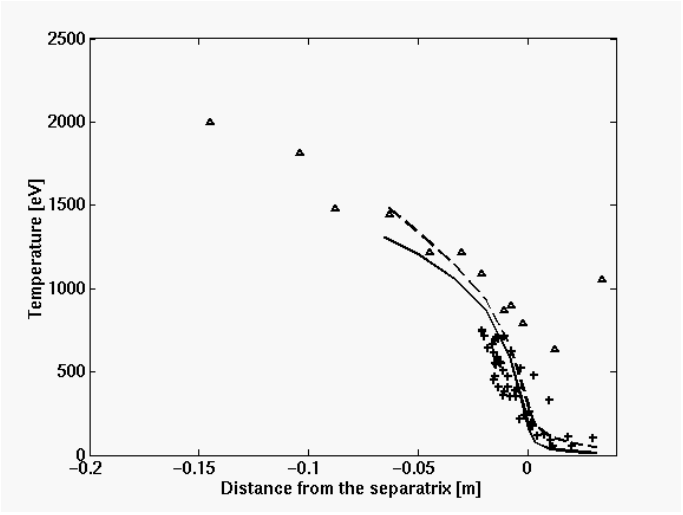

Figure 4. Electron and ion temperature profiles from numerical modeling and different experimental diagnostics. (+) edge lidar T_e, (—) numerical model T_e, (□) charge exchange T_i, (--) numerical model T_i.

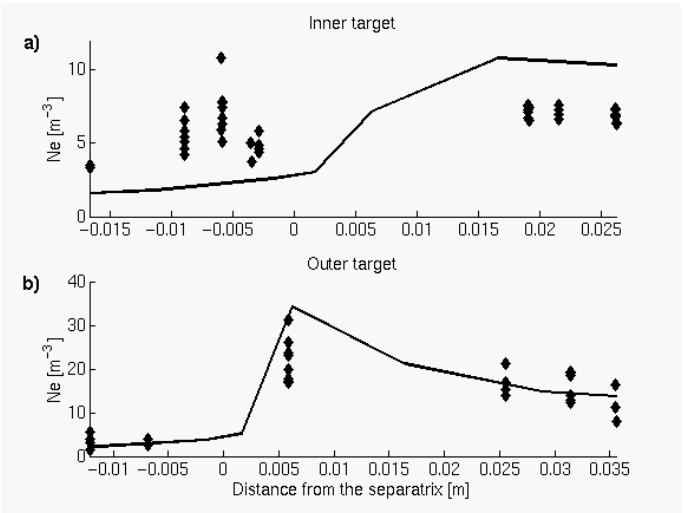

Figure 5. Electron density target profiles. (—) Numerical model, (♦) Langmuir probes data. a) inner target, b) outer target.

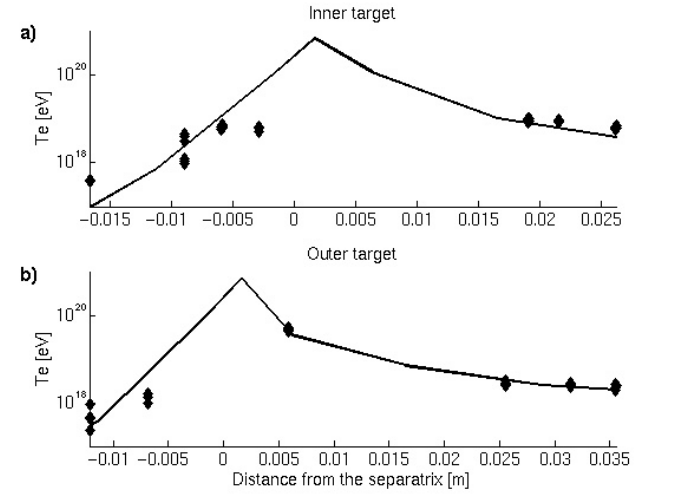

Figure 6. Electron temperature target profiles. (—) Numerical model, (♦) Langmuir probes data. a) inner target, b) outer target.

coupled in the inner plasma for the parameters we are considering. Modelling is consistent with this hypothesis.

We complete the analysis of the steady-state model with the electron density (figure 5) and temperature (figure 6) at the target plates, compared with experimental data from an array of Langmuir probes. The measurements show a large scatter, as is often the case for Langmuir probes. In addition, the number of available experimental points is low. This is due to the low data acquisition system frequency (100 Hz) and the short time window (*Dt=30* ms), selected to have data unaffected by the periodic occurrence of ELMs. Figures (3)-(6) show that our modelling of the steady-state phase is consistent with the experimental data to within a factor 2. We accept this result, considering the uncertainties in the measurements and the theoretical model.

Transient (ELM)

Table 1 compares the numerical duration of the trigger used for the ELM with the experimental data available for the case we selected. We choose the duration based on fast measurements of magnetic activity. The resulting energy loss reproduces satisfactorily the experimental estimate. Particle losses are over-estimated, but still consistent with the large measurement uncertainties.

In Figure 7 we show the heat flux profiles at the targets, taken at the times of the peak arrival. Two preliminary experimental estimates are reported. Our model is in rough agreement with the measurements at the outer target, while seems to under-estimate the experimental values at the inner one. The modelled peak value is consistent in order of magnitude with the upper measurement at the outer target and the lower one at the inner. The numerical model predicts a sharp decay of the flux in the private region, which seems not present in the experiment. We are investigating the reason of this disagreement.

Finally, in Figure 8 we compare the times of the peak heat fluxes at the targets as measured and modelled. In both cases the peak heat flux at the outer target precedes the inner one, consistently with the theoretical models, which predict the energy losses to happen preferentially at the outer side [9]. The agreement in the measured and modelled delay between the targets is about 25%. For the experimental data, we plotted the minimum energy flux estimate at the inner target and the maximum at the outer. This choice does not influence the temporal location of the peaks.

Table 1. Data for ELM trigger

	Measured value	**Modelled value**
Trigger duration [s]	□6×10^{-4}	6×10^{-4}
Particle losses	1.4×10^{20}	2.3×10^{20}
Energy losses [J]	2.3×10^{5}	2.4×10^{5}

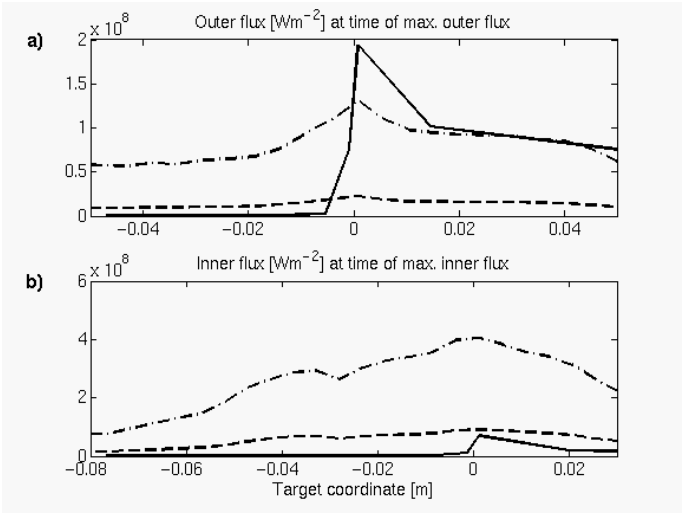

Figure 7. Target heat fluxes. a) outer target, b) inner target. For each target, profiles are shown at the time of the maximum peak value. Two different estimates are presented for the experimental data. (—) Numerical model, (--) lower experimental value, (-.-.) upper experimental value. By convention, the private region has negative spatial coordinate.

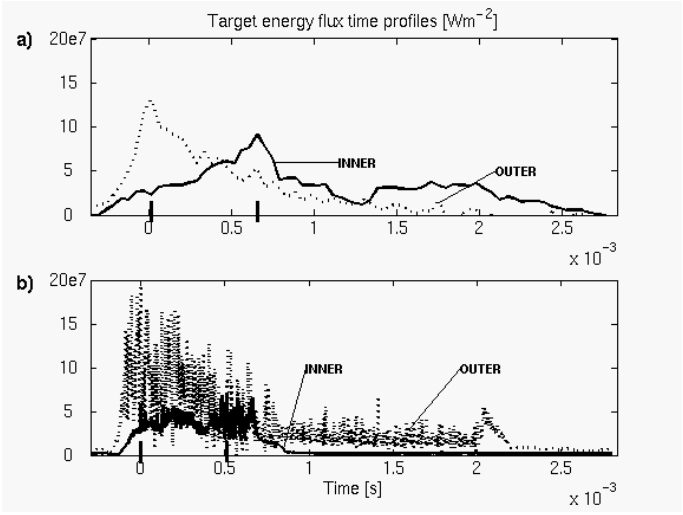

Figure 8. Heat flux evolution at (—) the inner and (…) the outer targets. a) experimental data, b) modeling results. The thick vertical ticks on the time axis mark the heat fluxe peaks. Note the noise in the computed traces, due to the statistical nature of the Monte Carlo method.

4. CONCLUSIONS

We presented a numerical model of an ELM in the JET tokamak. We were able to simulate the quiescent inter-ELM phase of the discharge with acceptable accuracy. It also was possible to reproduce qualitatively some global characteristic of an ELM. However, some fine details of the event are not correctly modelled with the current techniques, with a larger discrepancy between the model and the measurements at the inner target.

In this work we concentrated on the analysis of the transient target heat fluxes. From an engineering point of view, the particle fluxes are as important as the heat fluxes, because the high energy ions hitting the targets can erode them quite effectively. Analysis of the target

particle fluxes generated by ELM events is currently ongoing, and should be included in a future work.

Numerical plasma modelling can help the designer to roughly predict the working conditions of a divertor during an ELM, but further effort is required to achieve high accuracy on the details.

5. ACKNOWLEDGEMNTS

F. Subba wishes to thank the *Associazione per lo Sviluppo scientifico e tecnologico del Piemonte* (ASP) for financial support during the preparation of this work.

6. NOMENCLATURE

$\overline{B}$	Magnetic field [T].
D	Particle diffusivity [$m^2 \cdot s^{-1}$].
$\hat{I}$	Unit tensor [-].
$\bar{j}$	Electric current density [$C \cdot m^{-2} \cdot s^{-1}$].
m^i	Ion mass [kg].
$n^{i(e)}$	Ion (electron) density [m^{-3}].
p	Pressure [pa].
$q^{i(e)}$	Ion (electron) energy flux [$J \cdot m^{-2} \cdot s^{-1}$].
$T^{i(e)}$	Ion (electron) temperature in energy units [J].
$S^{E,i(e)}$	Ion (electron) energy source [$J \cdot m^{-3} \cdot s^{-1}$].
S^i	Ion particle source [$m^{-3} \cdot s^{-1}$].
$S^{\Gamma,i}$	Ion momentum source [$kg \cdot m^{-2} \cdot s^{-2}$].
t	Time [s].
$\overline{V}^i$	Ion velocity [$m \cdot s^{-1}$].
$V^i_{//}$	Ion velocity along the magnetic field [$m \cdot s^{-1}$].
$\hbar^i$	Ion viscosity [$kg \cdot m^{-1} \cdot s^{-1}$]
j	Electric potential [V].
$\overline{\Gamma}^i$	Ion flux [$m^{-2} \cdot s^{-1}$].
$\Gamma^i_{//}$	Ion flux along the magnetic field [$m^{-2} \cdot s^{-1}$].
c	Energy diffusivity [$m^2 \cdot s^{-1}$].
t_{ion}	Ionisation time [s].

7. REFERENCES

1. ITER Physics Basis Editors, et al., special issue of *Nuclear Fusion*, vol. 39, Chap. 1, Overview and Summary, 1999.
2. T. Eich, et al., Power Deposition Measurements in Deuterium and Helium Discharges in JET MKIIGB Divertor by IR-Thermography, *Jour. Nucl. Mater.*, vols. 313-316, pp. 919-924, 2003.
3. A. Loarte, et al., ELM Energy and Particle Losses and their Extrapolation to Burning Plasma Experiments, *Jour. Nucl. Mater.*, vols. 313-316, pp. 962-966.
4. R. Zanino, et al., Numerical Simulation of a 2-D Conduction-convection-radiation Model Problem in Divertor Geometry Using Adaptive Finite Elements, *Czechoslovak Journal of Physic*, vol 48, suppl. S2, pp 351-356, 1998.
5. F. Subba and R. Zanino, A 2-D Fluid Model of the Scrape-off Layer (SOL) Using Adaptive Unstructured Finite Volumes, *Jour. Nucl. Mater*, vols. 290-293, pp 743-747, 2001.
6. X.Bonnin, et al., Improved Modelling of Detachment and Neutral-dominated Regimes Using the SOLPS B2-Eirene Code, *Jour. Nucl. Mater*, vols. 313-316, pp. 909-913, 2003.
7. J.P. Freidberg, Ideal Magneto-Hydro-Dynamics, Plenum Press, New York, 1987, chap. 2.
8. S.I. Braginskii, Transport Processes in a Plasma, in M.A. Leontovich (ed.), Reviews of Plasma Physics, vol. 1, Consultants Bureau, New York, 1965, p. 205.
9. P.C. Stangeby, The Plasma Boundary of Magnetic Fusion Devices, Institute of Physics Publishing, Bristol and Philadelphia, 2000, chaps. 1, 3, 6, 16.
10. V. Rozhansky, et al., B2-solps5.0: SOL Transport Code With Drifts and Currents, *Contrib. Plasma Phys.*, vol. 40, pp. 328-333, 2000.
11. V. Rozhansky, et al., Impact of E×B Drifts on the Distribution of Impurities in the Tokamak Plasma Edge, *Jour. Nucl. Mater*, vols. 313-316, pp. 1141-1149, 2003.
12. S.V. Patankar, Numerical Heat transfer and Fluid Flow, Hemisphere, New York, 1980.
13. D. Reiter, et al., Time Dependent Neutral Gas Transport in Tokamak Edge Plasmas, *Jour. Nucl. Mater*, vols. 220-222, pp. 987-992, 1995.
14. V. Rozhansky, et al., Perpendicular Conductivity and Self Consistent Electric Fields in Tokamak Edge Plasmas, *Contrib. Plasma Phys.*, vol. 40, pp. 423-430, 2000.
15. H. Zohm, Edge Localized Modes (ELMs), *Plasma Phys. Control. Fusion*, vol 38, pp. 105-128, 1996.